

Behavioral phenotypes of SCN-specific Dicer knockout mice

Ngoc-Hien Du¹, Konstantinos Kompotis¹, Miho Sato¹, and Steven Brown¹

¹University of Zurich

August 29, 2024

Abstract

The suprachiasmatic nucleus (SCN) is the master clock that orchestrates circadian clocks across the body to synchronize with and anticipate the earth's light/dark cycles. Although post-transcriptional regulators called microRNAs have been implicated in physiological SCN function, how the absence of the entire mature miRNome impacts SCN output has not yet been explored. Here, we have generated an SCN-specific Dicer knockout mouse model by crossing Syt10Cre mice with Dicerflox mice to study behavioral consequences of miRNA depletion in the SCN. We show that loss of all mature miRNAs in the SCN shortens the circadian period length by ~40 minutes at the tissue level, and by ~50 minutes at the locomotor activity level. Knockout animals also showed arrhythmicity or ultradian locomotor activities with no light masking under constant light, a condition which usually caused lengthening of the circadian period length and reduced activities, i.e. light masking, in nocturnal animals. Moreover, induction of Dicer knockout by Cre injection into the SCN of adult Dicerflox mice eventually resulted in loss of behavioral rhythms. Finally, we show suggestive evidence that SCN desynchronization might be one mechanism underlying the behavioral phenotypes of SCN-specific Dicer knockout animals.

1 **Title page**

2

3 **Behavioral phenotypes of SCN-specific *Dicer* knockout mice**

4 Ngoc-Hien Du^{1*}, Konstantinos Kompotis¹, Miho Sato¹, and Steven Brown¹

5 ¹Institute of Pharmacology and Toxicology, University of Zurich, 8057 Zurich,
6 Switzerland

7 *Correspondance: Ngoc-Hien Du, hiendngoc@gmail.com, ORCID iD: 0009-0007-
8 3525-8094.

9 Present address: Ngoc-Hien Du, Laboratory for Biomedical Microfluidics, Swiss
10 Federal Institute of Technology Lausanne (EPFL), Rue du Bugnon 25A, 1005
11 Lausanne, Switzerland.

12 **Keywords:** SCN-specific *Dicer* knockout, miRNAs, locomotor activity, period length,
13 circadian rhythms

14 **Acknowledgements:** NH. D. designed and performed the study. K. K. performed
15 the injections for the inducible knockout model. M. S. performed the immunostaining
16 experiments. NH. D. carried out the analysis. NH. D., K. K., and M. S. wrote the
17 manuscript. We thank Sara Pierre for helping with the MEA recording. We thank
18 Professor David Gatfield for providing the *Dicer*<sup>fl^{ox} mice as well as infrastructure to
19 carry out part of the wheel running experiments. We thank Professor Steven Brown
20 for the supervision of the project and mentorship.</sup>

21 **Conflict of interest disclosure:** The authors declare no conflict of interest.

22

23

24

25

26

27

28

29

30

31

32 Abstract

33 The suprachiasmatic nucleus (SCN) is the master clock that orchestrates circadian
34 clocks across the body to synchronize with and anticipate the earth's light/dark
35 cycles. Although post-transcriptional regulators called microRNAs have been
36 implicated in physiological SCN function, how the absence of the entire mature
37 miRNome impacts SCN output has not yet been explored. Here, we have generated
38 an SCN-specific *Dicer* knockout mouse model by crossing *Syt10^{Cre}* mice with
39 *Dicer^{flox}* mice to study behavioral consequences of miRNA depletion in the SCN. We
40 show that loss of all mature miRNAs in the SCN shortens the circadian period length
41 by ~40 minutes at the tissue level, and by ~50 minutes at the locomotor activity level.
42 Knockout animals also showed arrhythmicity or ultradian locomotor activities with no
43 light masking under constant light, a condition which usually caused lengthening of
44 the circadian period length and reduced activities, i.e. light masking, in nocturnal
45 animals. Moreover, induction of *Dicer* knockout by Cre injection into the SCN of
46 adult *Dicer^{flox}* mice eventually resulted in loss of behavioral rhythms. Finally, we
47 show suggestive evidence that SCN desynchronization might be one mechanism
48 underlying the behavioral phenotypes of SCN-specific *Dicer* knockout animals.

49

50 Introduction

51 Circadian rhythmicity relies on a hierarchical system of clocks coordinated by a
52 master clock residing in the brain region called the suprachiasmatic nucleus (SCN)¹.
53 This small nucleus lies just above the optic chiasm, and receives direct photic
54 information from the ganglion cells of the retina². The master clock then
55 orchestrates peripheral clocks throughout the organism to synchronize with the
56 environment^{3,4}. At the organismal levels, the circadian clocks exert their function on
57 vital behaviors such as sleep/wake cycles, and feeding/fasting rhythms⁴. At the
58 molecular level, the output of all autonomous clocks is rhythmic gene expression
59 with a period of about 24 hours⁵. Interestingly, a large proportion of the
60 transcriptome, ~43% in mouse⁶, 44% in human⁷, and 82% in primate⁸, is rhythmically
61 expressed somewhere in the body.

62 Circadian gene expression originates not only from circadian transcription, but also
63 from circadian post-transcriptional and post-translational mechanisms^{9,10}. A recent
64 meta-analysis and modeling approach estimated that 30% of circadian transcripts
65 are regulated post-transcriptionally in mouse liver¹¹. Among the known post-
66 transcriptional mechanisms, the short (19-25 nucleotides) non-coding RNA
67 molecules coined microRNAs (miRNAs) play a crucial role in shaping the dynamics
68 of gene expression, by regulating both mRNA degradation and translation of a
69 multitude of target genes. There are more than 1000 miRNA genes in the human
70 genome that target up to 60% of protein coding genes^{12,13}, with one miRNA targeting
71 from a dozen to hundreds of mRNA targets¹⁴. In the last two decades, miRNAs have
72 emerged as important players in regulating all kinds of biological processes,
73 including circadian rhythms, from the molecular to the behavioral level.

74 The involvement of miRNAs in circadian oscillations has been reported in cell lines¹⁵,
75 in peripheral tissues¹⁶, as well as in the SCN^{17,18}. However, most studies focus on
76 the role of an individual miRNA in a specific context. Informative as it may be, this
77 approach often cannot showcase the magnitude of miRNA influence on a biological
78 system. We previously demonstrated a comprehensive view of miRNA regulation of
79 the hepatic transcriptome employing a genetic mouse model in which miRNA
80 biosynthesis was inactivated (liver-specific *Dicer* knockout)¹⁹. In our hands, miRNAs
81 played an essential role in adjusting the phase and amplitude of 30% of the circadian
82 transcriptome in mouse liver.

83 To study the roles of miRNA ensemble in shaping the function of the master clock,
84 we have now extended the use of tissue-specific *Dicer* knockout model from the liver
85 to the SCN. We report here that the SCN-specific *Dicer* knockout variably altered
86 both tissue and behavioral circadian period length in two different mouse models.
87 We also provide suggestive evidence that should be taken into consideration in
88 future investigations of the molecular mechanisms underlying the behavioral
89 phenotypes.

90

91 **Materials and Methods**

92 **Animals**

93 All animal experiments were performed according to the cantonal guidelines of either
94 the Canton of Vaud, Switzerland, license 2376.1, or the Canton of Zurich,
95 Switzerland, license 060/2017. Animals were allowed to access food and water *ad*
96 *libitum* under a 12:12-hr light dark (LD) cycle, unless otherwise stated. *Dicer^{flox}* mice
97 (IMSR_JAX:006366) were gift from Professor David Gatfield¹⁹, *Syt10^{Cre}* knock-in
98 mice (MGI:5286607) were gift from Dr. Henrik Oster²⁰, *Period2::Luciferase*
99 (*Per2::Luc*) knock-in mice (MGI:3040876) were gift from Dr. Joseph Takahashi²¹.
100 Genotype of the animals were examined by PCR as described in the original
101 publication of each mouse strain. Due to the expression of *Syt10* in the testis, males
102 homozygous for *Syt10^{Cre}* should not be used for mating. Male of genotype *Dicer*
103 *flox/flox*; *Syt10^{Cre} +/+* were crossed with female *Dicer flox/flox*; *Syt10^{Cre} KI/+* to create
104 knockout of genotype *Dicer flox/flox*; *Syt10^{Cre} KI/+* and control of genotype *Dicer*
105 *flox/flox*; *Syt10^{Cre} +/+*. Animals aged between 2-6 months were used for the
106 experiments. Litter mates or animals of similar ages were used for the same
107 experimental conditions.

108

109 **Genotyping**

110 Polymerase chain reaction (PCR) was used for genomic DNA extracted from either
111 the tail, ear or olfactory bulb to genotype each tissue or animal. To genotype alleles
112 of *Dicer*, the following two primers were used: DicerR1,
113 AAACATGACTCTTCAACTCAAACCTCAAACG, and DicerF1,
114 AATATTAATCCTGACAGTGACGGTCCAAAG. To confirm deletion of exon 23,
115 primer DicerF1 and DicerDel, GGGCAGCCCCATCTCAAAGGCCTACCTGAG were

116 used. To genotype alleles of *Syt10*, the following three primers were used: Syt10 F,
117 AGACCTGGCAGCAGCGTCCGTTGG; Syt10 R,
118 AAGATAAGCTCCAGCCAGGAAGTC; Syt10 KI,
119 GGCGAGGCAGGCCAGATCTCCTGTG. To genotype alleles of *Per2::Luc*, the
120 following three primers were used: P1, CTGTGTTTACTGCGAGAGT; P2,
121 GGGTCCATGTGATTAGAAAC; P3, TAAAACCGGGAGGTAGATGAGA.

122

123 **Tissue explants and bioluminescence recording and analysis**

124 *Dicer^{fllox}*; *Syt10^{Cre}* mice were crossed to *Per2::Luc* mice for bioluminescence
125 recording of tissue explants. To prepare tissue explants, animals were sacrificed,
126 and each tissue was collected into ice-cold HBSS (Cat# 14025, Life Technologies,
127 CA) with 10 mM Hepes (Cat# H0887, Sigma, MO). For SCN and pituitary, brains
128 were sliced at 300 µm interval with a McILWAIN Tissue Chopper, and each area was
129 isolated separately in ice-cold HBSS buffer with Hepes. For kidney, liver, tail and
130 lung, pieces of tissues were sliced at 300 µm interval. Each tissue explant was
131 cultured on either millicell (#PICMORG, Merckmillipore, MA) or a piece of hydrophilic
132 PTFE-membrane (#BGCM00010, Merckmillipore, MA) submerged with DMEM (Cat#
133 D2902, Sigma, MO) with 0.035 % Sodium bicarbonate (Cat# S8761, Sigma, MO), 10
134 mM Hepes (Cat# H0887, Sigma, MO), 4.5 g/L D-glucose (Cat# G8769, Sigma, MO),
135 1.0 % Penicillin-Streptomycin (Cat# 15070-063, Life Technologies, CA), 2% B27
136 (Cat# 17504044, Gibco) and 0.1 mM D-Luciferin (Promega, WI). Circadian
137 bioluminescence was recorded with photomultiplier tubes (PMTs) every 48 mins at
138 34.5 °C with 5% CO₂. To assess period length of the bioluminescence *ex vivo*, the
139 original data were subtracted with 24-hr running average and sinusoidal curve fitting
140 was applied using Lumicycle analysis software (Actimetrics).

141

142 **Locomotor activity recordings and analysis**

143 Mice were individually housed in cages containing running wheels, or with infrared
144 detectors as indicated, with *ad libitum* access to food and water. Data was collected
145 and analyzed using ClockLab software (Actimetrics). For jetlag experiment, onset
146 was extracted using ClockLab software, and the phase shift half time, defined as the
147 time at which half the phase shift was completed was extracted using *drda R*
148 package²².

149

150 **Immunohistochemistry**

151 Animals were deeply anaesthetized with Pentobarbital and intracardially perfused
152 with 10 ml of ice-cold saline, followed by 20 ml of ice-cold 4% paraformaldehyde /
153 0.1 M phosphate buffer (PB, pH 7.4). Brains were collected and post fixed in 4%
154 paraformaldehyde with 0.1 M PB for overnight at 4 °C followed by cryoprotection in
155 20% sucrose / 0.1 M PB for 48 hrs at 4 °C. The brains were sectioned by 30 µm with
156 cryostat at -17 °C and washed in 0.1 M PB at room temperature. The sections were
157 treated with 5% goat serum, incubated either with or without 1:1000 primary antibody

158 (α -Vip (Cat# T-4246, Peninsula laboratories, RRID: AB_518682) with 2% NGS in
159 PBS with 0.05% Triton (PBS-Triton), rinsed in PBS and PBS-Triton, incubated with
160 1:1000 secondary antibody (Goat α -Rabbit IgG labelled with Cy3, Cat# ab6939,
161 abcam, RRID: AB_955021) with 2% NGS in PBS-Triton, and then rinsed in PBS and
162 PBS-Triton. The sections were mounted onto gelatin-coated microscope slides, air-
163 dried, and dehydrated with Fluoromount™ Aqueous Mounting Medium (Cat# S3023,
164 Dako). Fluorescent images were obtained with a widefield microscope Apotome
165 (Zeiss, Germany).

166

167 **Multi-electrode recordings and analysis**

168 Mice were sacrificed and brains were quickly removed at ZT2 (ZT0 is light on time,
169 ZT12 is light off time). Brains were sliced coronally with the vibratome (#7000smz-2,
170 Campden Instruments) by 300 μ m in ice cold artificial cerebro-spinal fluid (ACSF, in
171 mM: NaCl 95; KCl 1.8; KH₂PO₄ 1.2; CaCl₂ 0.5; MgSO₄ 7; NaHCO₃ 26; glucose 15;
172 sucrose 50; oxygenated with 95% O₂; 5% CO₂; pH 7.4, measured osmolarity 310
173 mosmol kg⁻¹). After 30 minutes incubation, a 300 μ m slice containing the SCN was
174 placed on a 60pMEA100/30iR-Ti-gr perforated array (Multi Channel Systems).
175 Slices were positioned so that the entire SCN was in contact with the electrode
176 region of the array, and kept in place with a weight, with suction from underneath to
177 maximize contact between the slice and the electrodes. Oxygenated ACSF at 34°C
178 ran continuously through the MEA chamber for the duration of the experiment
179 (1.2ml/min inflow / 17ml/min outflow + gravity flow inflow/suction outflow at 65). Field
180 potential was detected by the MEA at 20,000 Hz using *Multi-Channel Experimenter*
181 (Multi Channel Systems). Data was recorded every 30 minutes. Because of the
182 large file size, recordings were limited to 10 minutes at the beginning of each 30
183 minutes for the duration of the experiment. Data were analyzed using Offline Sorter
184 (Plexon) as follows: files were run through a butterworth high pass filter at 300 Hz
185 and 'spikes' were detected using a threshold of ± 4 Standard Deviations. For each
186 spike the waveform was analyzed and a unit assigned to each unique waveform
187 detected from an individual electrode using the Valley Seeking spike sorting
188 algorithm. Spikes were distinguished from noise by waveform. Data were analyzed
189 using NeuroExplorer v5. Only spikes with mean frequency > 0.5 Hz were used.
190

191 **Injection of AAV constructs expressing *hSyn-Cre* in the SCN**

192 Male *Dicer^{flox}* mice (12-16 weeks old) were stereotactically (Kopf Instruments, CA,
193 USA) injected under isoflurane anesthesia, bilaterally at the SCN (ML= ± 0.18 mm;
194 AP= 0.46 mm; DV= 5.8 mm; relative to bregma). The following viruses were injected
195 at a volume of 300 nl with a rate of 150 nl/min: For knockouts (n=6), ssAAV9/2-
196 hSyn1-chl-mCherry_2A_iCre-WPRE-SV40p(A) (UZH Vector Core, 7.9x10¹² viral
197 particles/ml; iCre: Addgene #24593) and for controls (n=7), ssAAV9/2-hSyn1-chl-
198 mCherry-WPRE-SV40p(A) (UZH Vector Core, 4.8x10¹² viral particles/ml). Post-
199 surgery, mice were returned to the housing cage, and allowed to recover. After the
200 passage of three weeks to ensure recombination and adequate expression of the
201 AAV constructs, locomotor activity (using running wheel) was recorded under various
202 light-dark conditions. Following the completion of the experiment, mice were

203 perfused with 4% paraformaldehyde (PFA), their brains extracted, and sites of
204 injection were confirmed through mCherry expression with confocal microscopy.
205 Mistargeted animals were excluded from further analyses.

206

207 **Results**

208 *Generation of SCN-specific miRNA depletion mouse model*

209 To study the function of miRNAs in the SCN, we generated a mouse model in which
210 miRNA biogenesis is inactivated in the majority of the SCN cells. We bred mice
211 carrying conditional knockout alleles for the *Dicer1* gene (referred to as *Dicer^{flox}* in
212 the following), and mice carrying *Cre* recombinase cDNA inserted into the
213 *Synaptotagmin 10* locus (referred to as *Syt10^{Cre}*), a gene strongly expressed in the
214 SCN²⁰, and obtained *Dicer^{flox}; Syt10^{Cre}* mice, called here SCN-specific *Dicer*
215 knockout (KO) mice. Due to the small size of the SCN and potential contamination
216 from surrounding tissues that limits its use in PCR analysis, the olfactory bulb, which
217 also expresses *Syt10*, was used for PCR analysis to confirm successful
218 recombination at the *Dicer^{flox}* locus (Figure S1). PCR analysis of the ear showed no
219 detection of the recombined allele as expected.

220

221 *SCN-specific Dicer knockout showed shorter free-running period with variable onsets*

222 We found that knockout animals had shorter free-running period than control animals
223 (Figure 1, knockout mean = 22.93 h, control mean = 23.78 h, $t_{\text{Welch}}(9.23) = 5.33$, $p =$
224 $4.35e-04$). Knockout animals also reentrained almost immediately to a new light-
225 dark cycle after 6 h phase advance (Figure 2A, C). Analysis of the phase shift half
226 time, i.e. time required to reach half of the phase shift, showed that knockout animals
227 required only 0.63 ± 0.60 days while controls required 2.37 ± 0.25 days to reach 3h
228 phase shift. There was a tendency of faster re-entrainment to 6 h phase delay in
229 knockout animals vs controls (Figure 2B, D). The delay phase shift half time was
230 0.31 ± 0.57 days and 0.76 ± 0.08 days for knockouts and controls, respectively. The
231 high variation for knockouts in the phase delay experiments was due to low mouse
232 number. It is noticeable that the standard deviation of phase shift half time was
233 higher in knockout than that in controls, due to apparently variable activity onsets, for
234 which we quantified further below.

235 We found that knockouts showed activity onsets that were different to light-off time
236 by 31.9 ± 12.1 minutes, while controls showed only 7.3 ± 5.2 minutes activity onset
237 differences (Figure 3A, $t_{\text{test}} p = 8.2e-05$). For the knockout animals, the differences
238 were mostly due to earlier wake-up while there were also occasions where the
239 animals showed activity onset after the light-off time. In addition to the less precise
240 activity onset time, knockout animals showed larger variation in their activity onsets
241 compared to control animals. Under LD = 12:12, the standard deviation of onset
242 time was 44.1 ± 20.3 minutes for knockouts and 6.1 ± 3.1 minutes for controls
243 (Figure 3B, $t_{\text{test}} p = 4.4e-05$). Since running wheel might change the animals'
244 behaviors, we measured onset in another cohort of animals using infrared detector

245 (Figure 3C, Figure S2). In spite of the difference in the devices, we found again that
246 knockout animals showed larger standard deviation of 43.6 ± 7.0 minutes in their
247 activity onsets, compared to 16.0 ± 8.4 minutes for controls (Figure 3C, ttest $p =$
248 $1.4e-04$). The large standard deviation in activity onsets of knockouts was consistent
249 with all tested 24-hour period light-dark conditions with different day length (Figure
250 4). Reasoning that shorter period length of knockout animals might enable easier
251 entrainment to shorter environmental cycles, we measured activity onset under LD =
252 11:11. Indeed, knockout animals showed smaller onset variation than controls
253 (Figure 3D, knockout = 0.97 ± 0.34 h, control = 2.35 ± 1.12 h, ttest $p = 0.038$).
254 These results suggest that, due to the shorter internal period length, it was more
255 challenging for knockout animals to get entrained to the light/dark cycles of 24 hours.
256 However, we cannot rule out that larger onset variation is due to defects in SCN
257 synchrony. Therefore, we next investigated knockout behaviors under conditions
258 that challenge SCN synchrony.

259

260 *Lack of miRNAs in the SCN caused arrhythmicity and lack of light masking under* 261 *constant light condition*

262 Since constant light condition (LL) has long been used to disrupt circadian rhythms²³,
263 mice lacking Dicer in their SCN were recorded under LL condition (Figure 5). We
264 observed that control animals under LL exhibited longer period length for the
265 duration tested (Figure 5B), whereas knockout animals showed arrhythmicity or
266 ultradian rhythms (Figure 5A). Unlike control animals, knockout animals did not
267 show light masking, i.e. reduced activities under constant light condition observed in
268 nocturnal animals. Increasing light intensity during the LL condition did not affect the
269 lack of the masking effect in knockout animals (data not shown). Interestingly,
270 knockout animals did show masking response at the beginning of the LD = 3:3
271 condition (Figure 6), an ultradian light condition that has been shown to disrupt
272 circadian rhythmicity²⁴. This suggests that knockout animals did not show light
273 masking response under constant light condition, despite remaining responsive to
274 light.

275

276 *SCN tissue explants from SCN-specific Dicer knockout also showed shorter period* 277 *length*

278 To confirm if the short circadian period in the behavior of knockout animals was due
279 to the disrupted SCN, we bred *Dicer^{flox}; Syt10^{Cre}* mice with *Period2::Luciferase*
280 (*Per2::Luc*) knock-in mice and cultured their tissue explants from different tissues
281 (Figure 7). Knockout tissue indeed showed shorter period length in an SCN-
282 dependent manner (Figure 7A, knockout SCN mean = 24.21 h, control SCN mean =
283 24.83 h). We also observed that pituitary from knockout animals showed shorter
284 period length (knockout pituitary mean = 23.76 h, control pituitary mean = 24.74 h),
285 as expected from the expression of *Syt10* in the pituitary²⁵. It is worth noting that
286 during SCN explant preparation, SCN from knockout animals detached more easily

287 from the optic chiasm, and the amplitude of PER2::LUC oscillations in the SCN
288 knockouts often damped faster than control slides (Figure 7B).

289

290 *Inducible SCN-specific Dicer knockout showed shorter period length that eventually*
291 *led to arrhythmicity*

292 To rule out the effect of extra-SCN expression of *Syt10*, as well as the effect of
293 possible developmental process, on the period length phenotype observed in our
294 knockout model, we induced *Dicer* knockout in the SCN by injecting AAV expressing
295 *hSyn-Cre* to the SCN. Two weeks after injection, behavioral phenotypes were
296 assessed by recording wheel running activities (Figure 8). We found that induced
297 knockout animals exhibited either directly arrhythmicity or a shorter period length that
298 eventually led to arrhythmicity under any of the light conditions tested.

299

300 *Indication that desynchronization might be one mechanism explaining the behavioral*
301 *phenotype of Dicer knockout animals*

302 We next sought the possible mechanisms underlying the behavioral phenotypes
303 observed in knockout animals. It has been previously demonstrated that the
304 vasoactive intestinal peptide (VIP), expressed in the SCN by a neuronal population
305 receiving first the photic stimulus from the retinal ganglion cells, is the main
306 synchronizer of the SCN neuronal networks²⁶. Therefore, investigating the
307 expression of VIP in the SCN of genetically *Dicer* knockout animals was the first
308 reasonable step. We found suggestive evidence that VIP expression was reduced in
309 the SCN upon depletion of miRNAs (Figure S3). Subsequently, we measured SCN
310 network synchronization by recording neuronal activity of brain slices on multi
311 electrode array (MEA). We found that only a portion of SCN from knockout retained
312 its firing ability, conversely to slices from control animals in which the whole SCN
313 fired in synchrony (Figure 9). Although these observations need to be recapitulated
314 in a larger number of animals, taken together they suggest that SCN
315 desynchronization may be one of the mechanisms underlying the behavioral
316 phenotypes observed in knockout animals.

317

318 *Gender differences observed in Dicer knockout animals*

319 We observed that knockout females reached extreme weight (Figure S4A at 13-
320 month-old, knockout females weighed 59.9 g, while control females weighed 32.7 g,
321 both n = 2). Knockout females were also less fertile. Over a period of one year,
322 from 10 breeding pairs between control males and knockout females, one pair
323 produced 4 litters, four pairs produced 2 litters, and five pairs produced only one litter
324 before pausing pregnancy. Regarding the circadian period, SCN tissue explants
325 from KO females showed shorter period compared to controls as in males (Figure
326 S4B, knockout SCN mean = 24.50 h, control SCN mean = 25.36 h). Surprisingly, we
327 found that tissue explants from pituitary gland of control females showed shorter
328 period compared to their SCN counterparts (control pituitary mean = 23.07 h), while

329 the two tissues from control males showed similar period (male pituitary mean =
330 24.74 h, male SCN mean = 24.83 h). In contrast, in knockout females, tissue
331 explants from pituitary gland exhibited similar period length (knockout female
332 pituitary mean = 24.33 h) compared to their SCN counterparts, as in males.

333

334 Discussion

335 In the current study, we explored the circadian consequences of depleting miRNAs
336 in the master clock of the mouse brain. We report here a shorter period length in
337 genetic knockout animals; and an initially variable, but finally arrhythmic, circadian
338 behavior in inducible adult knockouts. One variable aspect between the two
339 knockout models that might account for the difference in the observed phenotypes is
340 the potentially incomplete deletion of *Dicer* in the SCN of the genetic knockouts.
341 Indeed, it was previously shown that when using a *Syt10^{Cre}* mouse model to obtain
342 SCN-specific *Bmal1* knockouts, BMAL1 expression was deleted in the SCN in a Cre
343 dose-dependent manner²⁰. However, due to the expression of *Syt10* in the testis
344 and that whole body *Dicer* knockout is embryonic lethal^{27,28}, it is not possible to
345 obtain tissue specific *Dicer* knockout mice that are homozygous for *Syt10^{Cre}*. We
346 suggest that the incomplete deletion of *Dicer* in the SCN can be confirmed by
347 performing *in situ* hybridization of *Dicer* in the SCN. Complete *Dicer* deletion might
348 then lead to cell apoptosis in the SCN as has been seen in excitatory forebrain
349 neuron-specific *Dicer* knockout model²⁹. Since SCN lesion animals are arrhythmic,
350 we cannot exclude that SCN cell death could explain the arrhythmic phenotype in the
351 inducible knockout model. Another possible mechanism explaining the difference
352 between genetic and induced knockouts is compensation by neuronal plasticity
353 during development. This can be confirmed, for example, by knocking out *Dicer* in
354 neonatal SCN slices by infection with AAV expressing *hSyn-Cre*.

355 Surprisingly, the genetic *Dicer* knockout also exhibited a female specific phenotype,
356 namely obesity and compromised fertility. As reported in the original paper²⁰ and
357 elsewhere, *Syt10* is highly expressed in the SCN, although it can be found also in
358 the olfactory bulb and in the pituitary^{20,25}. Therefore, we cannot rule out that the
359 expression of *Syt10* outside of the SCN contributed to the above female *Dicer*
360 knockout phenotypes. Furthermore, we found that wild-type female mice's tissue
361 explants from pituitary showed shorter period length compared to the SCN tissue
362 explants from the same animals, a phenotype that was not observed in wild-type
363 males. In fact, gender differences in circadian phenotypes has been described
364 previously. For example, females re-entrain to new light-dark cycle rapidly at
365 proestrus than at metestrus³⁰. The fast re-entrainment of locomotor activity is
366 accompanied with fast clock phase shifts in peripheral tissues but not the SCN. The
367 observed phenotypes could be conveyed also via pro-opiomelanocortin (POMC)
368 neurons, which receive direct input from the SCN, and have been previously
369 implicated both in hyperphagia and obesity³¹, as well as sexually dimorphic functions
370 in the context of energy homeostasis³². Future studies should explore the
371 relationship between SCN and extra-SCN regions when using *Syt10^{Cre}* mouse
372 model, in both males and females.

373 *Dicer* knockout animals exhibited faster entrainment to a new light/dark cycle, which
374 is a phenotype observed also in mice lacking two vasopressin receptors V1a and
375 V1b³³ or LIM homeobox transcription factor Lhx1³⁴. In both vasopressin receptors
376 and Lhx1 deficient model, reduced interneuron coupling is the molecular mechanism
377 underlying the lack of resistance to a new light/dark cycle. These are aligned to our
378 suggestive evidence that SCN desynchronization is the cause for the behavioral
379 phenotypes. However, experiments with more animals need to be done to confirm
380 the reduced VIP expression as well as reduced firing rate in the SCN of knockout
381 animals. In the cortex, VIP is a predicted target of miR-28-3p³⁵. While miR-28-3p is
382 expressed in olfactory bulb, hippocampus, striatum, and the spinal cord, it is not
383 expressed in the cortex, where VIP is highly expressed. The reduction of VIP
384 expression in the *Dicer* knockout SCN therefore, could be an indirect consequence
385 of miRNA depletion. Further investigation of the underlying mechanism(s) should
386 examine the role of neuropeptide communication in the observed phenotypes. For
387 example, grafting control SCN onto knockout SCN might be able to rescue the
388 period length phenotypes.

389 Finally, determining the responsible miRNA(s) is crucial to understand miRNA-
390 dependent regulation of the SCN network. Recently, whole body deficiency in miR-
391 183/96/182 cluster was shown to affect locomotor activity as well as circadian
392 oscillations at tissue levels³⁶. However, in this mouse model, even though the mice
393 are behaviorally arrhythmic under constant darkness, SCN tissue explants are
394 rhythmic with the same period length as controls. Taking into consideration that
395 miR183/96/182 cluster was inactivated throughout the whole body, it is therefore
396 highly unlikely that they are driving the behavioral alterations observed in our *Dicer*
397 deficient models. Nevertheless, several miRNAs, such as miR-219³⁷, miR-132³⁷,
398 and miR-17³⁸, have recently been reported to be expressed rhythmically in the SCN.
399 miR-7a, whose predicted targets include *GABA B receptor 1*, and *Cry2*, is reported
400 to be enriched in the SCN³⁹. It might be that a combination of several SCN-specific
401 miRNAs regulates the master clock's activities. miRNAs and transcriptomic profiling
402 upon miRNA depletion in the SCN will help to answer the open questions.

403

404 **References**

- 405 1. Moore, R. Y. Organization of the mammalian circadian system. *Ciba Found.*
406 *Symp.* **183**, 86–88 (1995).
- 407 2. Abrahamson, E. E. & Moore, R. Y. Suprachiasmatic nucleus in the mouse:
408 Retinal innervation, intrinsic organization and efferent projections. *Brain Res.*
409 **916**, 172–191 (2001).
- 410 3. Weaver, D. R. The suprachiasmatic nucleus: a 25-year retrospective. *J. Biol.*
411 *Rhythms* **13**, 100–112 (1998).
- 412 4. Patton, A. P. & Hastings, M. H. The Mammalian Circadian Time-Keeping
413 System. *J. Huntingtons. Dis.* **12**, 91–104 (2023).
- 414 5. Partch, C. L., Green, C. B. & Takahashi, J. S. Molecular architecture of the
415 mammalian circadian clock. *Trends Cell Biol.* **24**, 90–99 (2014).

- 416 6. Zhang, R., Lahens, N. F., Ballance, H. I., Hughes, M. E. & Hogenesch, J. B. A
417 circadian gene expression atlas in mammals: Implications for biology and
418 medicine. *Proc. Natl. Acad. Sci.* 2–7 (2014) doi:10.1073/pnas.1408886111.
- 419 7. Ruben, M. D. *et al.* A database of tissue-specific rhythmically expressed
420 human genes has potential applications in circadian medicine. *Sci. Transl.*
421 *Med.* **10**, 1–8 (2018).
- 422 8. Mure, L. S. *et al.* Diurnal transcriptome atlas of a primate across major neural
423 and peripheral tissues. *Science (80-)*. **359**, (2018).
- 424 9. Crosby, P. & Partch, C. L. New insights into non-transcriptional regulation of
425 mammalian core clock proteins. *J. Cell Sci.* **133**, (2020).
- 426 10. Anna, G. & Kannan, N. N. Post-transcriptional modulators and mediators of the
427 circadian clock. *Chronobiol. Int.* **38**, 1244–1261 (2021).
- 428 11. Lück, S., Thurley, K., Thaben, P. F. & Westermarck, P. O. Rhythmic
429 Degradation Explains and Unifies Circadian Transcriptome and Proteome
430 Data. *Cell Rep.* 741–751 (2014) doi:10.1016/j.celrep.2014.09.021.
- 431 12. Krol, J., Loedige, I. & Filipowicz, W. The widespread regulation of microRNA
432 biogenesis, function and decay. *Nat. Rev. Genet.* **11**, 597–610 (2010).
- 433 13. Helwak, A., Kudla, G., Dudnakova, T. & Tollervey, D. Mapping the human
434 miRNA interactome by CLASH reveals frequent noncanonical binding. *Cell*
435 **153**, 654–65 (2013).
- 436 14. Liu, W. & Wang, X. Prediction of functional microRNA targets by integrative
437 modeling of microRNA binding and target expression data. *Genome Biol.* **20**,
438 18 (2019).
- 439 15. Park, I. *et al.* microRNA-25 as a novel modulator of circadian Period2 gene
440 oscillation. *Exp. Mol. Med.* **52**, 1614–1626 (2020).
- 441 16. Xu, S., Witmer, P. D., Lumayag, S., Kovacs, B. & Valle, D. MicroRNA (miRNA)
442 transcriptome of mouse retina and identification of a sensory organ-specific
443 miRNA cluster. *J. Biol. Chem.* **282**, 25053–66 (2007).
- 444 17. Alvarez-Saavedra, M. *et al.* miRNA-132 orchestrates chromatin remodeling
445 and translational control of the circadian clock. *Hum. Mol. Genet.* **20**, 731–51
446 (2011).
- 447 18. Mehta, N. & Cheng, H. Y. M. Micro-managing the circadian clock: The role of
448 microRNAs in biological timekeeping. *J. Mol. Biol.* **425**, 3609–3624 (2013).
- 449 19. Du, N.-H., Arpat, A. B., De Matos, M. & Gatfield, D. MicroRNAs shape
450 circadian hepatic gene expression on a transcriptome-wide scale. *Elife* **3**,
451 e02510 (2014).
- 452 20. Husse, J., Zhou, X., Shostak, A., Oster, H. & Eichele, G. Synaptotagmin10-
453 Cre, a driver to disrupt clock genes in the SCN. *J. Biol. Rhythms* **26**, 379–89
454 (2011).
- 455 21. Yoo, S.-H. *et al.* PERIOD2::LUCIFERASE real-time reporting of circadian
456 dynamics reveals persistent circadian oscillations in mouse peripheral tissues.

- 457 *Proc. Natl. Acad. Sci. U. S. A.* **101**, 5339–46 (2004).
- 458 22. Malyutina, A., Tang, J. & Pessia, A. *drda*: An R Package for Dose-Response
459 Data Analysis Using Logistic Functions. *J. Stat. Softw.* **106**, 1–26 (2023).
- 460 23. Ohta, H., Yamazaki, S. & McMahon, D. G. Constant light desynchronizes
461 mammalian clock neurons. *Nat. Neurosci.* **8**, 267–269 (2005).
- 462 24. Oishi, K., Higo-Yamamoto, S., Yamamoto, S. & Yasumoto, Y. Disrupted light-
463 dark cycle abolishes circadian expression of peripheral clock genes without
464 inducing behavioral arrhythmicity in mice. *Biochem. Biophys. Res. Commun.*
465 **458**, 256–261 (2015).
- 466 25. Roper, L. K., Briguglio, J. S., Evans, C. S., Jackson, M. B. & Chapman, E. R.
467 Sex-specific regulation of follicle-stimulating hormone secretion by
468 synaptotagmin 9. *Nat. Commun.* **6**, 8645 (2015).
- 469 26. Ono, D., Honma, K.-I. & Honma, S. Roles of Neuropeptides, VIP and AVP, in
470 the Mammalian Central Circadian Clock. *Front. Neurosci.* **15**, 650154 (2021).
- 471 27. Bernstein, E. *et al.* Dicer is essential for mouse development. *Nat. Genet.* **35**,
472 215–7 (2003).
- 473 28. Chen, R., D’Alessandro, M. & Lee, C. miRNAs Are Required for Generating a
474 Time Delay Critical for the Circadian Oscillator. *Curr. Biol.* 1–10 (2013)
475 doi:10.1016/j.cub.2013.08.005.
- 476 29. Davis, T. H. *et al.* Conditional loss of Dicer disrupts cellular and tissue
477 morphogenesis in the cortex and hippocampus. *J. Neurosci.* **28**, 4322–30
478 (2008).
- 479 30. Pilonis, V. J., Kolms, B. & Oster, H. Rapid Jetlag Resetting of Behavioral,
480 Physiological, and Molecular Rhythms in Proestrous Female Mice. *J. Biol.*
481 *Rhythms* **35**, 612–627 (2020).
- 482 31. Jais, A. *et al.* PNOCARC Neurons Promote Hyperphagia and Obesity upon
483 High-Fat-Diet Feeding. *Neuron* **106**, 1009-1025.e10 (2020).
- 484 32. Wang, C. *et al.* TAp63 contributes to sexual dimorphism in POMC neuron
485 functions and energy homeostasis. *Nat. Commun.* **9**, 1544 (2018).
- 486 33. Yamaguchi, Y. *et al.* Mice genetically deficient in vasopressin V1a and V1b
487 receptors are resistant to jet lag. *Science (80-.)*. **342**, 85–90 (2013).
- 488 34. Hatori, M. *et al.* Lhx1 maintains synchrony among circadian oscillator neurons
489 of the SCN. *Elife* **3**, e03357 (2014).
- 490 35. Soula, A. *et al.* Small RNA-Seq reveals novel miRNAs shaping the
491 transcriptomic identity of rat brain structures. *Life Sci. alliance* **1**, e201800018
492 (2018).
- 493 36. Zhou, L. *et al.* A genome-wide microRNA screen identifies the microRNA-
494 183/96/182 cluster as a modulator of circadian rhythms. *Proc. Natl. Acad. Sci.*
495 *U. S. A.* **118**, 1–9 (2021).
- 496 37. Cheng, H.-Y. M. *et al.* microRNA modulation of circadian-clock period and
497 entrainment. *Neuron* **54**, 813–29 (2007).

- 498 38. Gao, Q., Zhou, L., Yang, S.-Y. & Cao, J.-M. A novel role of microRNA 17-5p in
499 the modulation of circadian rhythm. *Sci. Rep.* **6**, 30070 (2016).
- 500 39. Herzer, S., Silahatoglu, A. & Meister, B. Locked Nucleic Acid-Based In Situ
501 Hybridisation Reveals miR-7a as a Hypothalamus-Enriched MicroRNA with a
502 Distinct Expression Pattern. *J. Neuroendocrinol.* **24**, 1492–1504 (2012).

503

504 **Figure legends**

505 Figure 1: SCN-specific *Dicer* KO had shorter period length. (A) Summary of free-
506 running period length under constant darkness (DD) measured by wheel running
507 activities. (B) Examples of two KO mice. (C) Examples of two control mice.

508 Figure 2: SCN-specific *Dicer* KO reentrained faster to jetlag. (A) Onset of locomotor
509 activities upon 6h-advanced jetlag at day 6 (control n = 10, KO n = 5, data is mean \pm
510 sem). (B) Onset of locomotor activities upon 6h-delayed jetlag at day 6 (control n =
511 5, KO n = 3, data is mean \pm sem). (C) Examples of advanced jetlag for KO mice.
512 (D) Examples of advanced jetlag for control mice.

513 Figure 3: KO mice had larger onset variation than controls. (A) Standard deviation of
514 onset time in minutes (measured from wheel running activities under LD = 12:12, KO
515 n = 5, ctrl n = 10, data = mean \pm sd). (B) Absolute difference to light off time in
516 minutes (measured from wheel running activities under LD = 12:12, KO n = 5, ctrl n =
517 10, data = mean \pm sd). (C) Standard deviation of onset time in minutes (measured
518 from infrared detector under LD = 12:12, KO n = 4, ctrl n = 9, data = mean \pm sd). (D)
519 Standard deviation of onset time in hours (measured from wheel running activities
520 under LD = 11:11, KO n = 4, ctrl n = 10, data = mean \pm sd).

521 Figure 4: KO mice adapted worse to different day length. (A) Examples of wheel
522 running activities from KO mice. (B) Examples of wheel running activities from
523 control mice.

524 Figure 5: KO mice had arrhythmic/ultradian rhythms in LL with no light masking. (A)
525 Examples of wheel running activities from KO mice. (B) Examples of wheel running
526 activities from control mice.

527 Figure 6: KO mice were masked by light to some extent under LD = 3:3 condition,
528 showing that the animals were not irresponsive to light. Animals were kept under DD
529 for 20 days before light conditions were changed as indicated in the figures.
530 Examples of wheel running activities from KO mice (A) and control (B).

531 Figure 7: SCN from KO mice also had shorter period length. (A) period length of *ex*
532 *vivo* culture of tissue slices from different tissues. (B) Examples of rhythms from
533 SCN and lung. SCN rhythms from KO mice were more difficult to obtain than those
534 from controls. Tissue explants from the same animals share the same colors.

535 Figure 8: When KO is induced by injection of *Dicer*^{flox} mice with AVV expressing
536 *hSyn-Cre*, KO mice had variable phenotypes, but eventually got arrhythmic. (A)
537 Control injection. (B) *hSyn-Cre* injection. Yellow part denotes when light was on.

538 Figure 9: Suggestive evidence of SCN firing being less synchronized in KO mice
539 than in control (n=1 each). SCN slides on MEA, annotation of electrodes that
540 overlapped with SCN region (purple circles), and SCN firing frequencies across time
541 points for KO (A) and control (B). Electrodes (6x10) are annotated as following: SCN
542 TRUE if the SCN is located above that electrode, SCN FALSE if not; MEA TRUE if
543 the electrode is technically functional, MEA FALSE if not. For the time series plots,
544 only electrodes that were located below the SCN and technically functional were
545 color-coded based on the firing frequencies.

546 Figure S1: Confirmation of recombination by PCR analysis. (A) Schematic of
547 genomic locus. Primers *DicerF1* and *DicerDel* produce a fragment of 601 nt length.
548 (B) Gel picture of the recombined *Dicer* fragment detected in the olfactory bulb of the
549 knockout (KO) animal but not in the ear.

550 Figure S2: Examples of onset detection in KO and control mice. Activities were
551 recorded using infrared detectors.

552 Figure S3: Example of VIP expression reduction in KO mice (ZT7, n=1). One should
553 note that the optical chiasm in the knockout SCN was not present in the slide,
554 indicating that one part of the SCN might have been ripped off.

555 Figure S4: Gender differences in phenotypes of knockout animals. (A) Female KO
556 were extremely overweighted. Left: control, right: KO female. (B) Period length of
557 tissue explants from control and KO females. Tissue explants from the same
558 animals share the same colors.

Figure 1

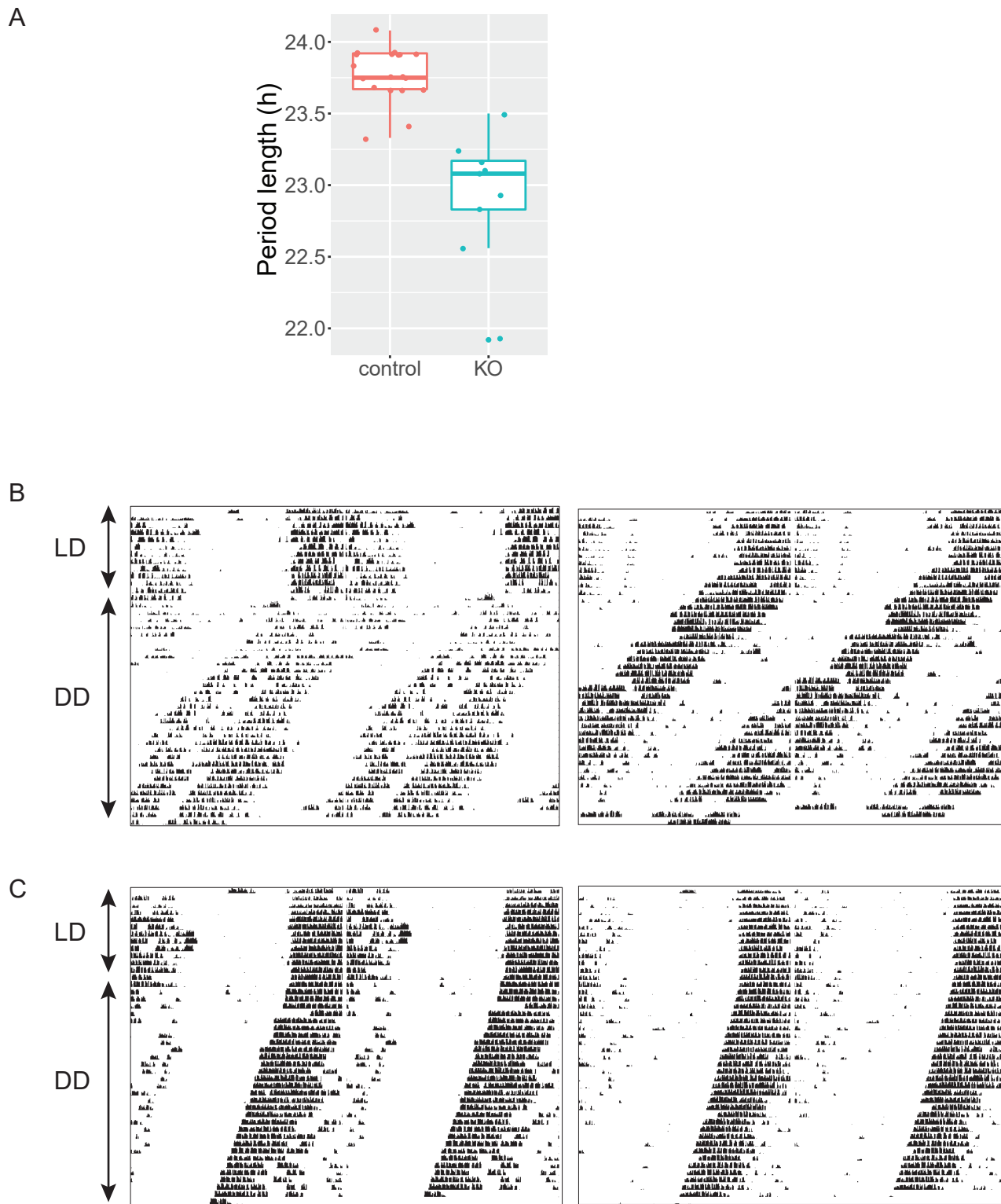


Figure 2

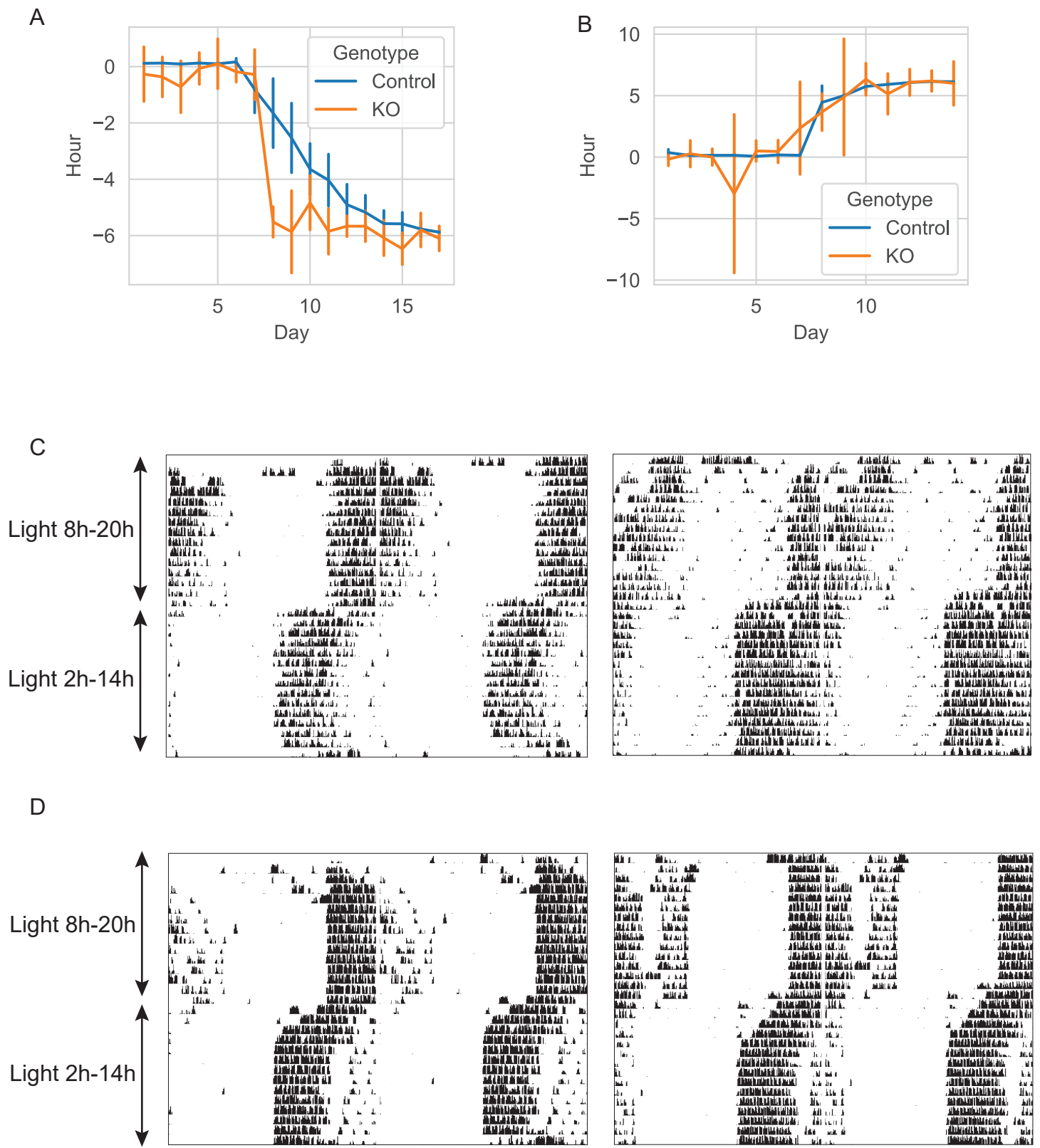
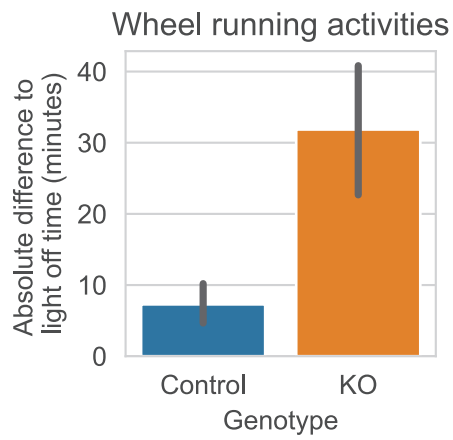
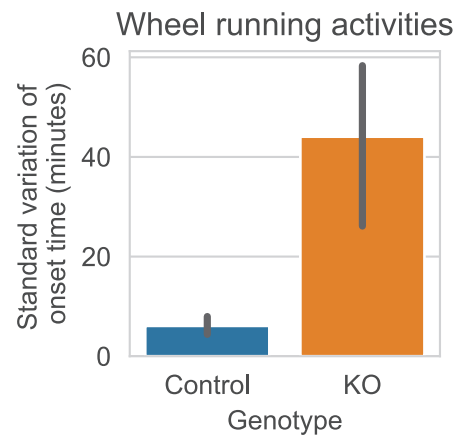


Figure 3

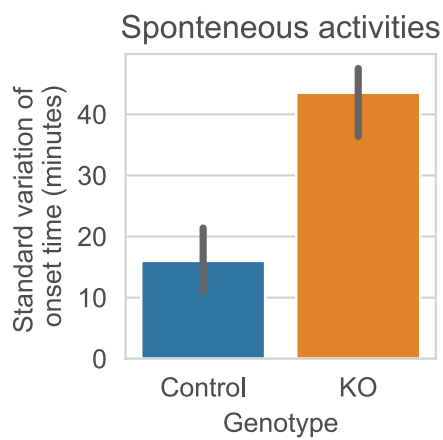
A



B



C



D

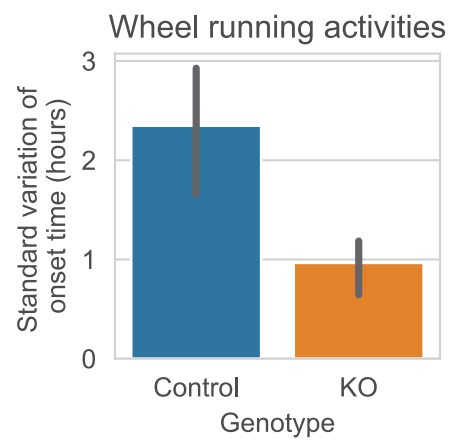
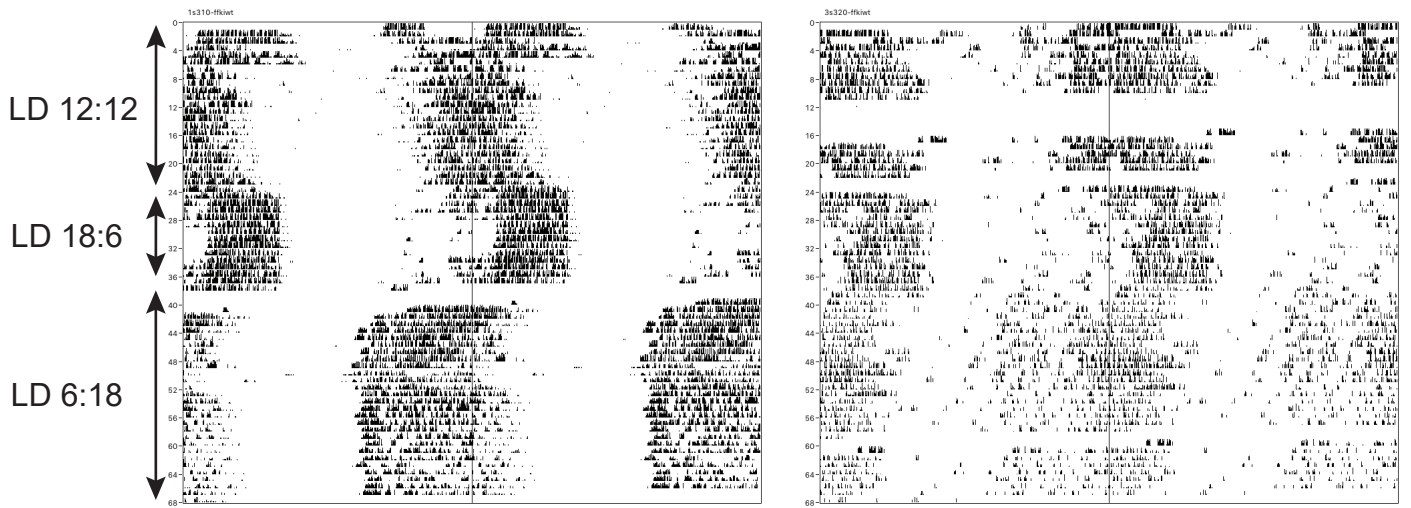


Figure 4

A



B

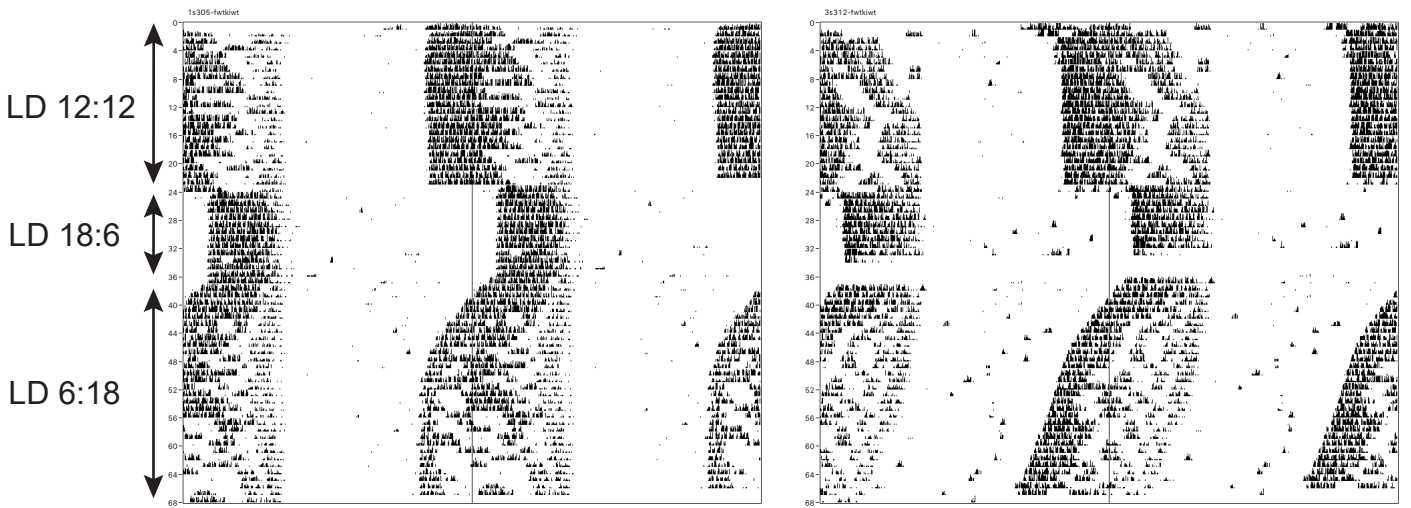


Figure 5

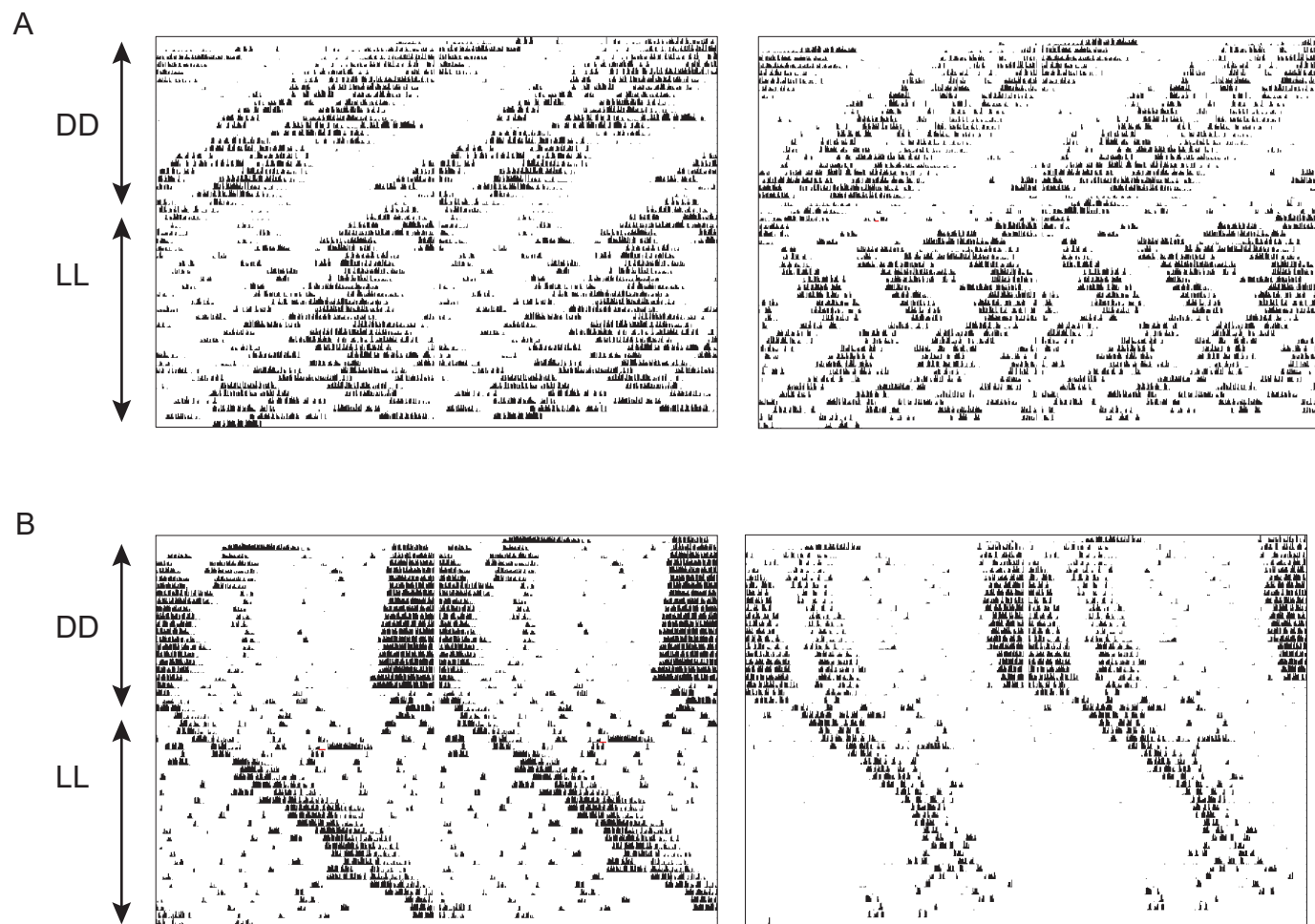


Figure 6

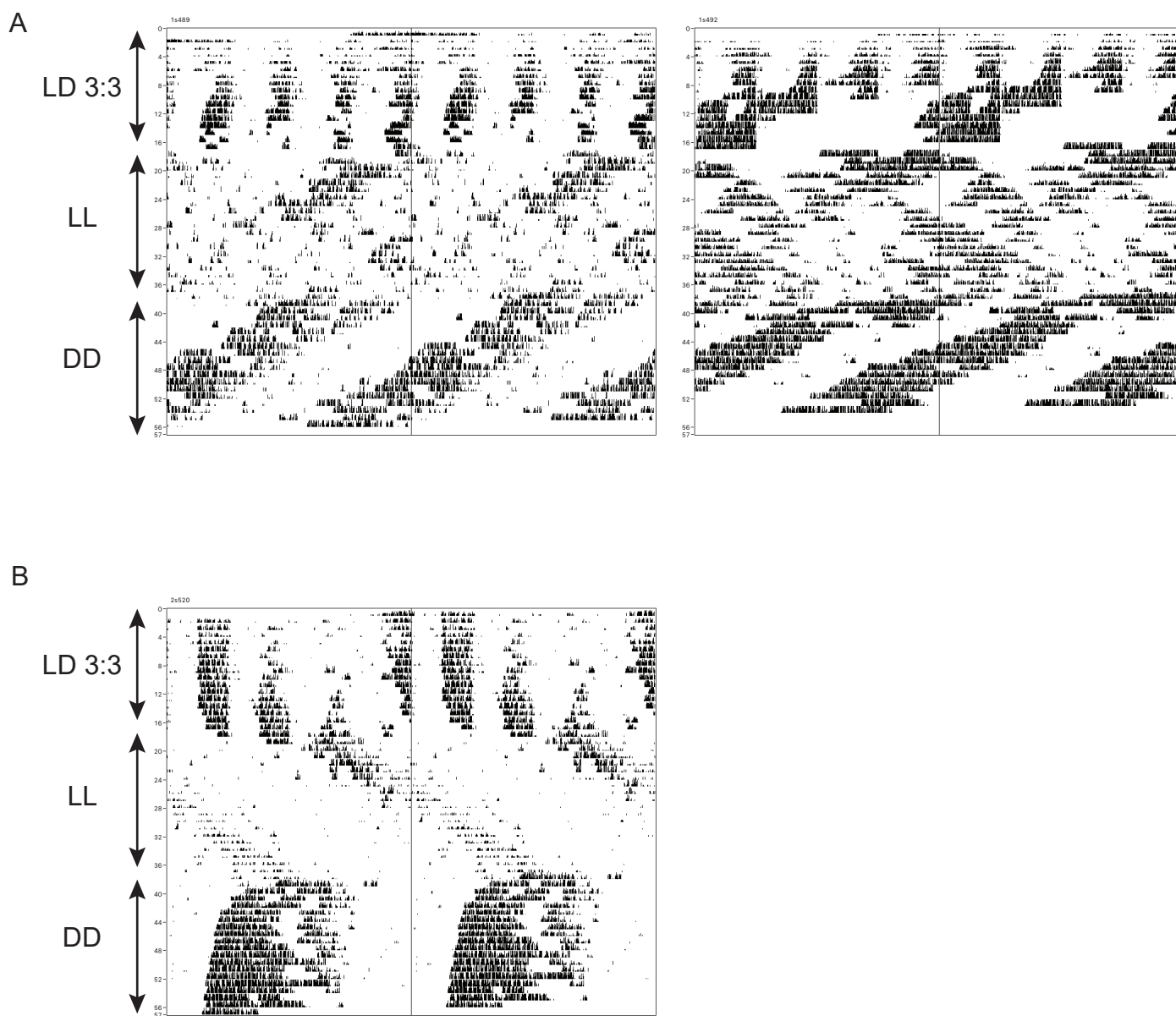
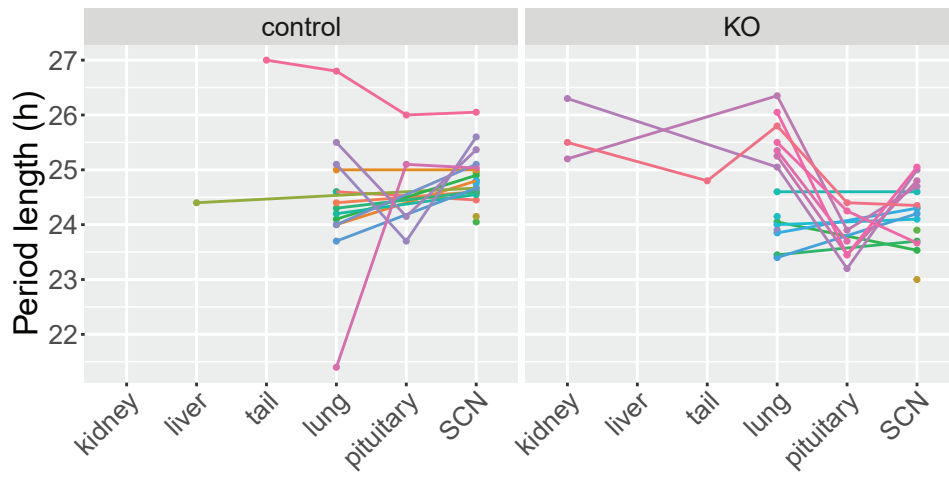


Figure 7

A



B

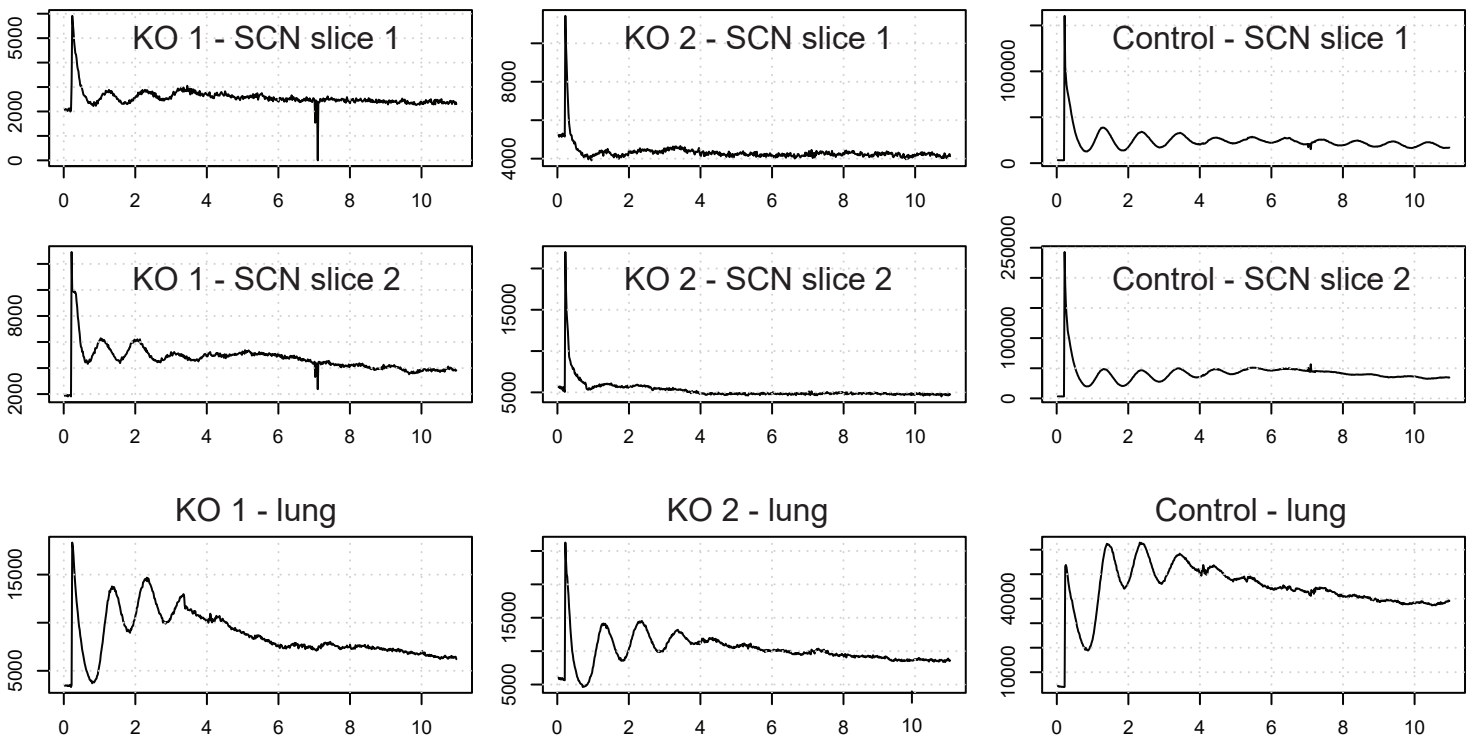


Figure 8

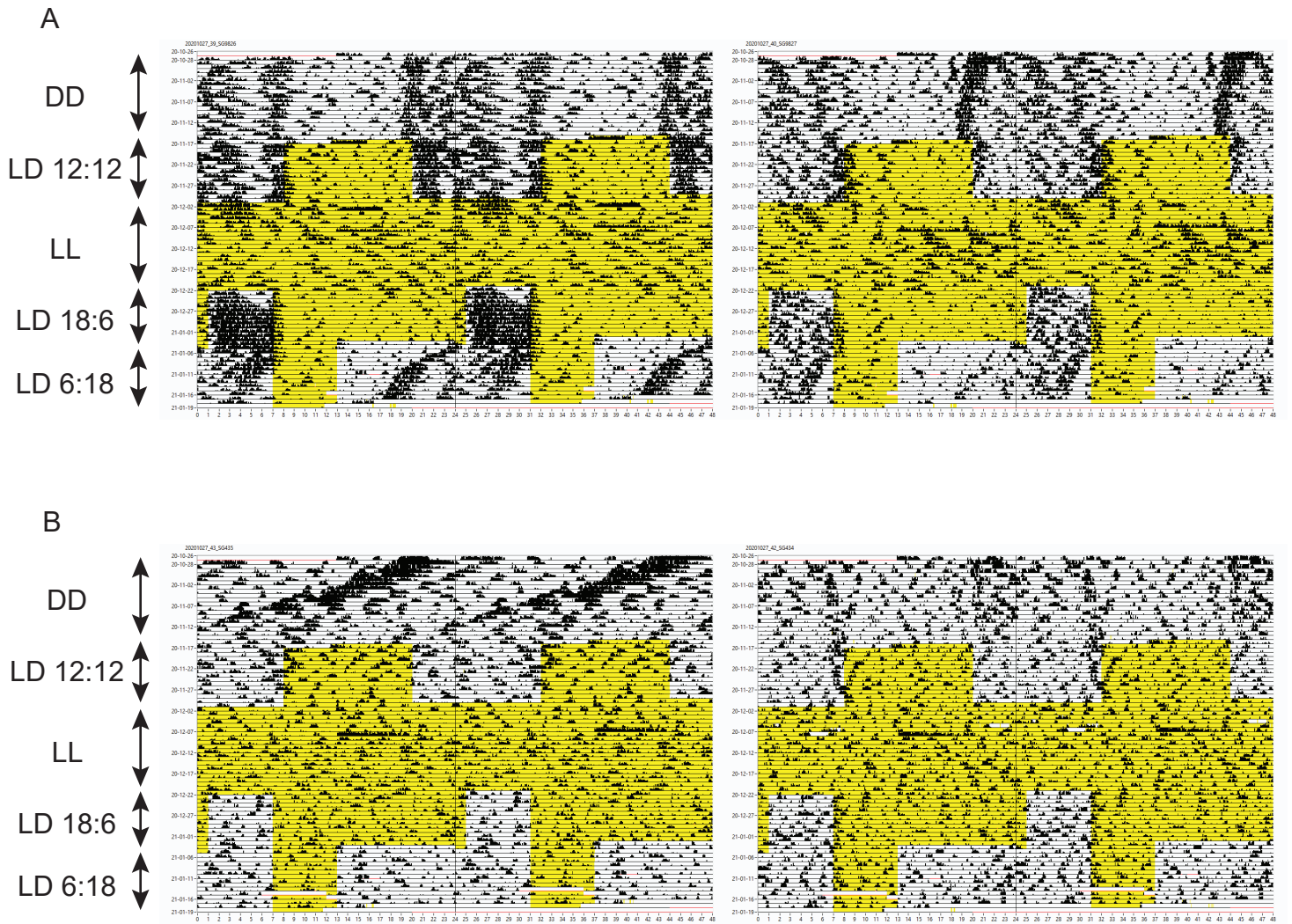
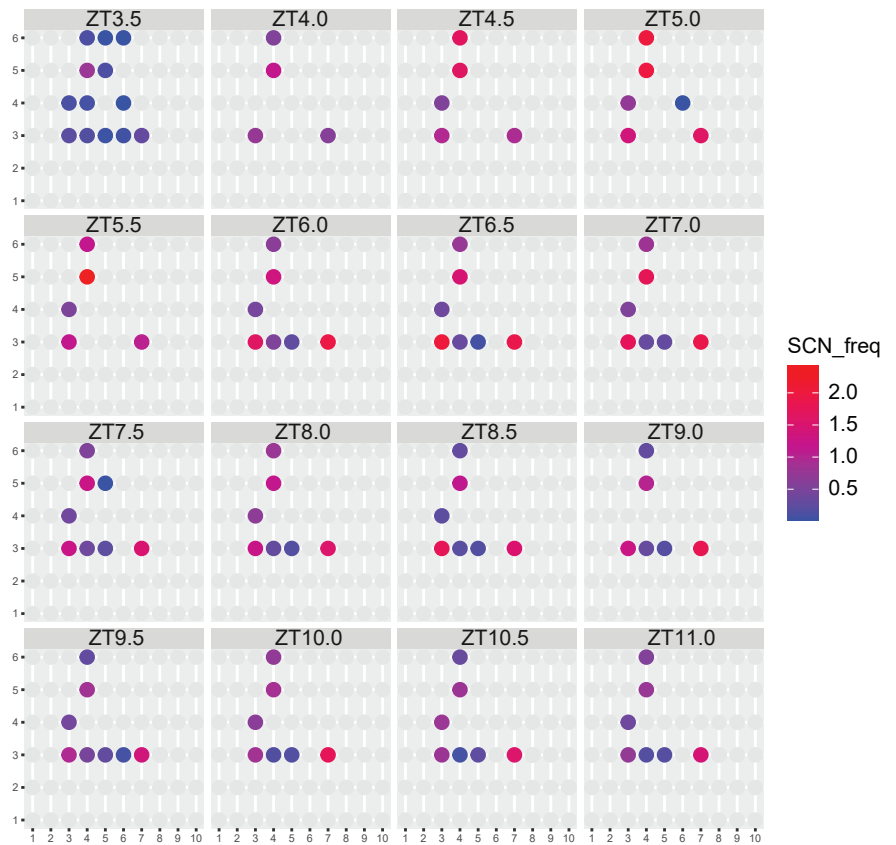
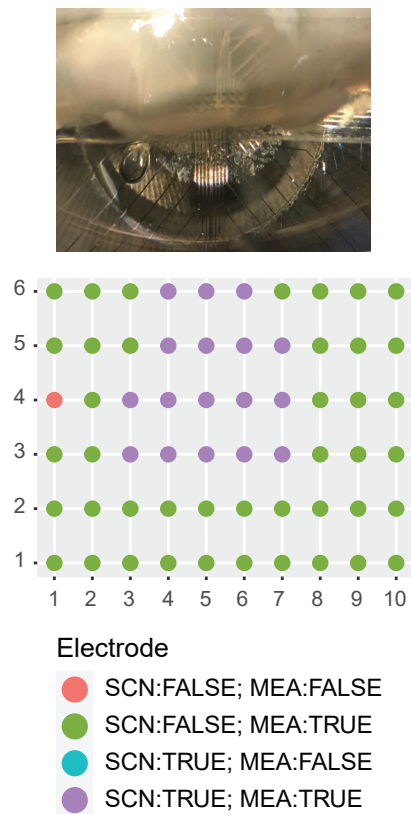


Figure 9

A



B

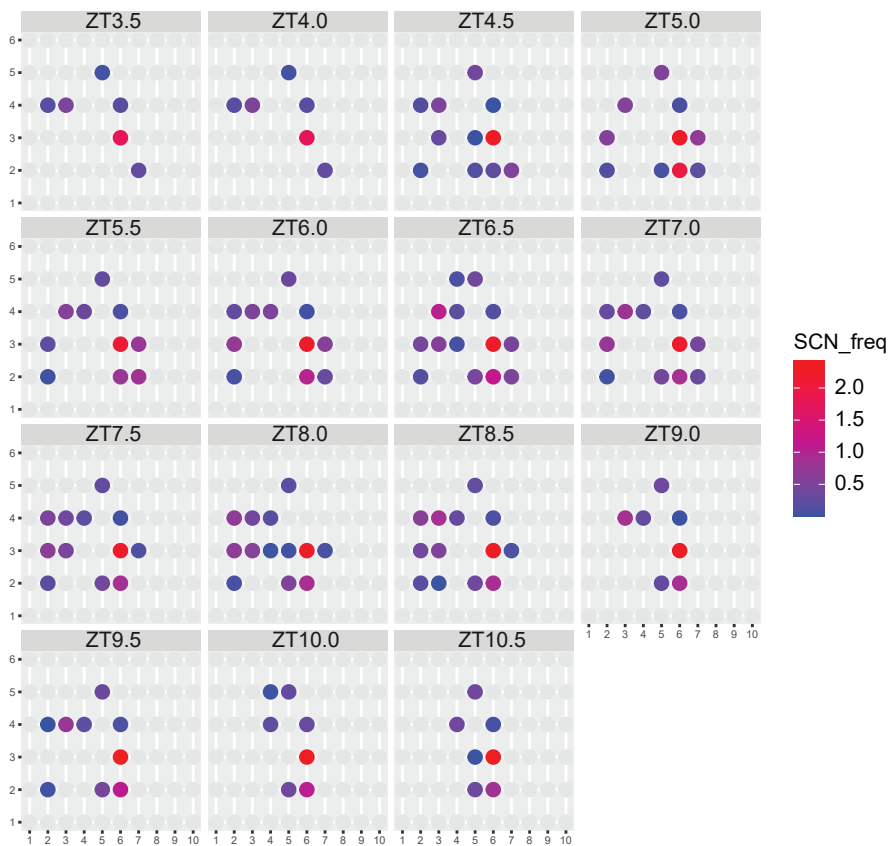
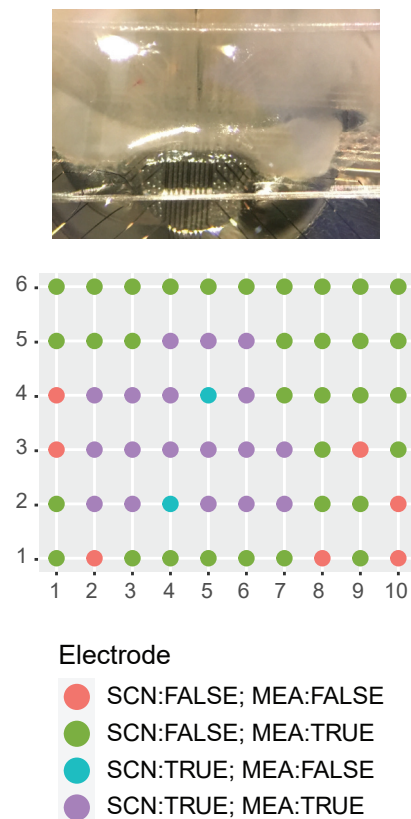
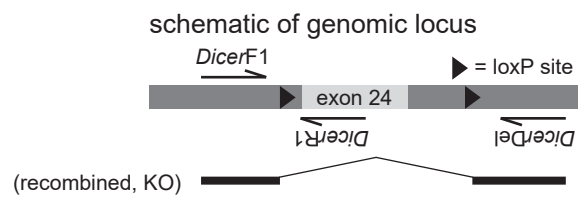


Figure S1

A



B

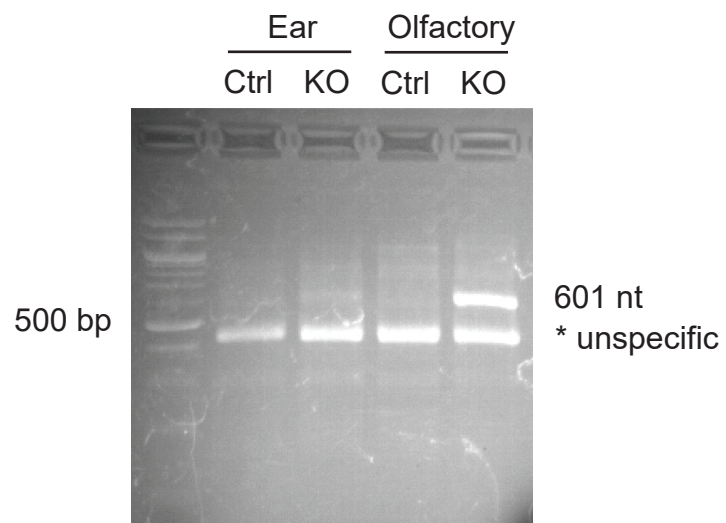
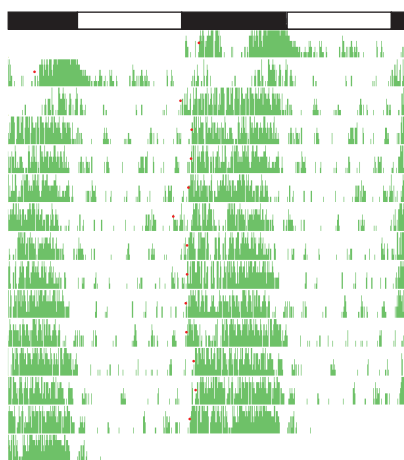
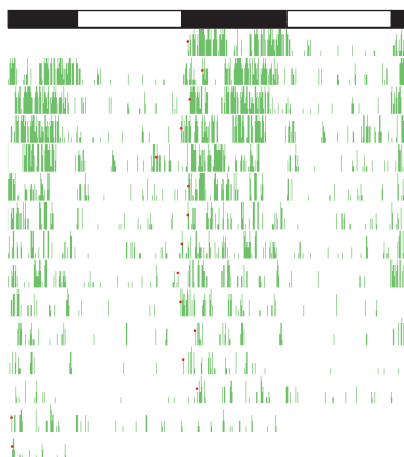
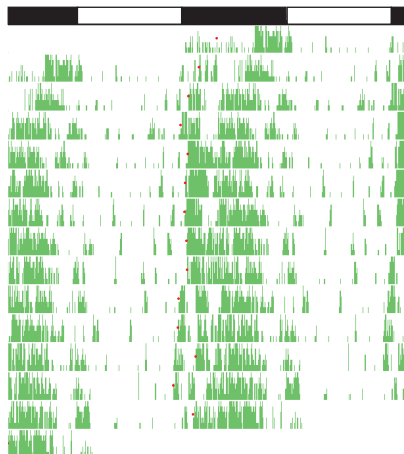


Figure S2

A



B

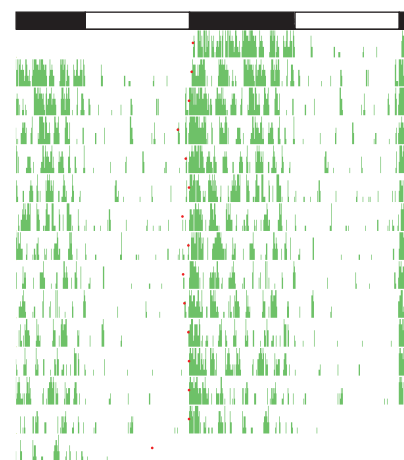
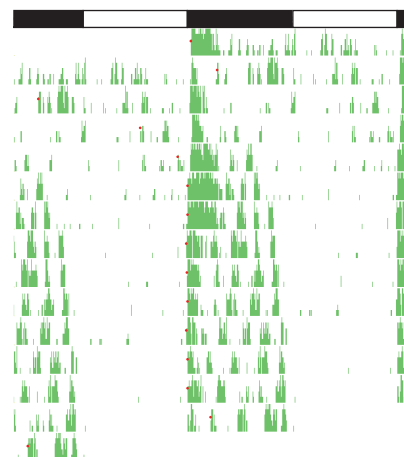
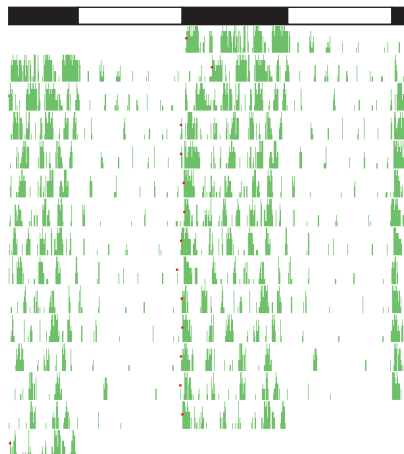


Figure S3

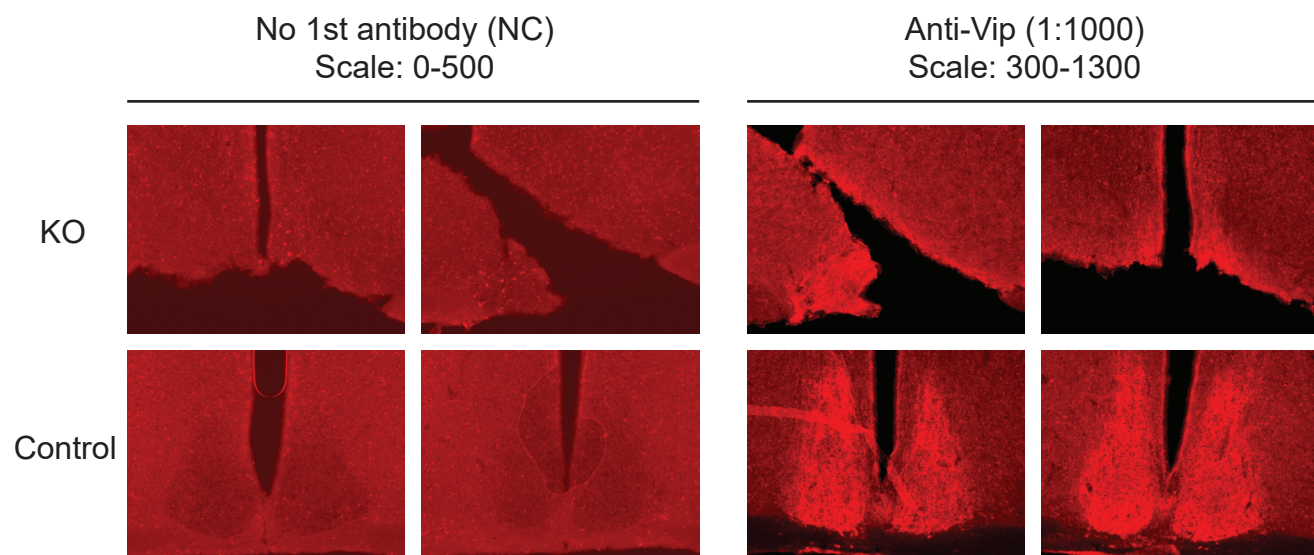


Figure S4

A



B

